Distributed Resilient Event-Triggered Control for Power Quality Improvement in Grid-Tied Microgrid Under Denial-of-Service Attack

Shengxuan Weng, Dong Yue, *Fellow, IEEE*, Jianbo Chen, and Chunxia Dou, *Senior Member, IEEE*

***Abstract*—This article proposes a distributed event-triggered control method for multifunctional grid-tied inverters (MFGTIs) in microgrid to improve power quality under denial-of-service (DoS) attack. The proposed method tackles two key challenges. The first is dynamic adjustment of inverter residual capacities responding to variations in the accessible renewable power and the harmonic and unbalanced current. The second is DoS-resistant event-triggered control with the following specific functional requirements in power quality improvement task. 1) Quantitative characterization and adjustability of convergence speed and accuracy. 2) Implementation based on sampled data with adjustable sampling period. 3) Reasonableness of DoS attack descriptions. 4) Guidance on selection of parameters. Theoretical analysis proves that the proposed method achieves adequate harmonic and unbalanced current compensation at the point of common coupling without wasting capacity and ensures fair utilization of all MFGTIs, even under DoS attacks. Simulation results further validate the effectiveness of the method.**

***Index Terms*—Denial-of-service (DoS) attack, distributed resilient control, event-triggered mechanism (ETM), multifunctional grid-tied inverter (MFGTI), power quality improvement.**

NOMENCLATURE

Variables and Parameters of Communication

L	Laplacian matrix of communication network.
a_{kj}	Weight of communication link between MFGTI$_k$ and MFGTI$_j$.
$\mathcal{A}(\tau,t)$	Attack interval in $[\tau,t)$.
$\mathcal{H}(\tau,t)$	Healthy interval in $[\tau,t)$.
$n(\tau,t)$	Number of OFF-to-ON transitions of DoS attack in $[\tau,t)$.
$\lvert\mathcal{A}(\tau,t)\rvert$	Duration of DoS attack in $[\tau,t)$.
η, T_f	DoS attack frequency constrained parameters.
κ, T_d	DoS attack duration constrained parameters.
$\overline{L}$	Matrix equals to $L+\text{diag}\{a_{10},a_{20},\ldots,a_{N0}\}$.
λ_2,λ_N	Second largest and maximum eigenvalues of L.
$\overline{\lambda}_1,\overline{\lambda}_N$	Minimum and maximum eigenvalues of $\overline{L}$.
$\lvert N_k\rvert$	Cardinal number of N_k.

Variables and Parameters of MFGTI

$i_{LC}(t)$	Harmonics and unbalanced current at time t.
$i_k^c(t)$	Compensation current reference of MFGTI$_k$ at time t.
I_k	Root-mean-square (rms) rated current of MFGTI$_k$.
I_k^a	Active part of I_k.
I_k^r	Reactive part of I_k.
ϕ_k	Active power factor of MFGTI$_k$.
$I_{\max}$	Maximum magnitude of i_{LC}.

Variables and Parameters of Control Algorithm

T_1	Individual residual capacity regulation period.
T_2	Total residual capacity estimation period.
T	Control flow period.
T_e	Event-detection period.
ϕ_0	Desired active power factor.
RC_k^{sum}	MFGTI$_k$'s estimated value about total residual capacity.
K,ε	Control parameters about ϕ_0.
K_1	Control parameters about ϕ_k.
a_{k0}	Information reception indicator of MFGTI$_k$ about ϕ_0.
$n_s^{\phi,k}T_e$	sth triggering time instant about ϕ_k.
$n_{s'(t)}^{\phi,j}T_e$	Latest triggering time instant about ϕ_j before time t.
α^{ϕ}	Parameters of event-triggered mechanism about ϕ_k.
K_2	Control parameters about RC_k^{sum}.
$n_s^{\text{RC},k}T_e$	sth triggering time instant about RC_k^{sum}.
$n_{s'(t)}^{\text{RC},j}T_e$	Latest triggering time instant about RC_j^{sum} before time t.
α^{RC}	Parameters of event-triggered mechanism about RC_k^{sum}.

Manuscript received 10 January 2023; revised 17 December 2023; accepted 15 February 2024. This work was supported in part by the National Natural Science Foundation of China under Grant 62293500, Grant 62073170, and Grant 62293505, and in part by the "1311 talent project" by Nanjing University of Posts and Telecommunications. *(Corresponding author: Shengxuan Weng.)*

The authors are with the Institute of Advanced Technology, Nanjing University of Posts and Telecommunications, Nanjing 210023, China (e-mail: shxweng@njupt.edu.cn; medongy@vip.163.com; jianbo686@aliyun.com; cxdou@ysu.edu.cn).

Digital Object Identifier 10.1109/JSYST.2024.3367307

I. INTRODUCTION

THE microgrid (MG) functions as a small-scale power system by integrating various renewable energy sources (RESs), energy storage, and local loads [1]. With widespread adoption of power electronics, substantial nonlinear and unbalanced loads have emerged. They inject harmonic and unbalanced current into the MG and the interconnected utility grid, which can degrade the operation of electrical equipment, introduce additional power losses, and cause instability [2]. Power quality improvement crucially involves compensating the harmonics and unbalanced current. The connection of RESs to the MG is facilitated through inverters with rated capacities [3]. Notably, these inverters often retain residual capacity, which proves valuable for compensating the harmonics and unbalanced current through power quality improvement functionality. This inverter, equipped with such capabilities, is referred to as multifunctional grid-tied inverter (MFGTI). The increasing penetration of MFGTIs, coupled with suitable control methods, presents advantages in reducing substantial investments in the maintenance and operation of conventional power quality mitigating devices [4].

Due to its flexibility, scalability, and plug-and-play functionality, the distributed control mode for power quality improvement in MFGTIs has gained considerable attention in recent years [5], [6], [7]. However, these studies assume that the residual capacity of the MFGTI is sufficient to improve power quality. Challenges arise when considering the stochastic variability in the accessible active power of RES, introducing uncertainty to the residual capacity. This uncertainty makes it difficult to ensure consistent fulfillment of compensation task under all circumstances, as observed in [8], where only partial harmonic current compensation can be realized under insufficient residual capacity. Addressing the allocation between active power and residual capacity of MFGTI, studies such as in [9] and [10] aim to achieve adequate compensation under insufficient residual capacity. However, these methods employ a centralized control architecture. Moreover, existing approaches lack proportionate sharing of tasks between active power generation and power quality improvement among all MFGTIs. In addition, there is no capability to dynamically adjust residual capacity based on real-time variations in accessible active power within each MFGTI and harmonic currents within MG. *These deficiencies presents the first challenge addressed in this study: designing a distributed control strategy for power quality improvement that dynamically adjusts the residual capacity of each MFGTI in response to variations in accessible active power and harmonic and unbalanced current. The proposed control method aims to achieve both adequate compensation and fair utilization across all MFGTIs.*

Due to communication resource limitation, the practical implementation of distributed control for power quality improvement based on continuous or periodic information transmission is hindered by high costs and potential traffic congestion [11]. Some studies, such as in [12], [13], have introduced event-triggered mechanism (ETM) to address this issue recently. These mechanism, extensively studied in multiagent systems and networked control systems, involve information transmission time instants triggered by predesigned conditions [14], [15], [16] aiming to achieve on-demand information transmission by reducing redundant information transfer. However, the widespread integration of information technology makes MG susceptible to denial-of-service (DoS) attack. Adversaries with limited knowledge of the target system can readily launch DoS attack to block the transmission of control and measurement data packets in the communication network [17], [18], [19]. The reduction in information redundancy caused by ETM renders the system more vulnerable to DoS attack, consequently leading to the failure of power quality improvement task. Despite our prior work [20] achieving adequate compensation and fair utilization across all MFGTIs under varying accessible active power, the method designed in that work is incapable of addressing the issues of DoS attack and communication resource limitation.

While some research work has explored the distributed event-triggered control of multiagent systems under DoS attack [21], [22], [23], [24], [25], applying these methods to power quality improvement presents challenges. This is due to the specific functional requirements associated with distributed event-triggered power quality improvement control under DoS attack scenarios as follows.

1) Quantitative characterization and adjustability of convergence speed and accuracy. Lacking this function can lead to inability of harmonics and unbalanced current to be compensated timely and accurately. This further results in injection of harmonics and unbalanced current into the MG and interconnected utility grid.
2) Implementation of ETM on sampled data with adjustable sampling period. Since information processing and transmission in MFGTI are physically realized using digital technologies, execution of ETM can only rely on sampled information rather than continuous information as in traditional mechanisms. Meanwhile, adjustability of sampling periods is needed due to computational capability limitations of MFGTI.
3) Reasonableness of DoS attack descriptions. The established DoS attack model should be general in capturing different attack scenarios. In addition, the assumptions on the constraints of DoS attack should not be overly stringent to realistically reflect real attack situations.
4) Guidance on selection of parameters. We need to provide a range for selecting parameters in both the control law and the ETM to meet power quality improvement operational requirements. Moreover, selection mechanisms for these parameters should be provided corresponding to different cases factors as the severity of attack, the degree of communication resource limitations, and the precision and speed requirements.

To the best of our knowledge, existing literature lacks a method that can simultaneously fulfill the four requirements mentioned previously. *These give rise to the second challenge addressed in this study: how to construct an effective control strategy under DoS attack that not only resolves the first challenge but also satisfies the four functional requirements mentioned previously while adhering to the principle of on-demand information transmission.*

Motivated by the above-mentioned analysis, this article attempts to develop distributed resilient event-triggered control method for MFGTIs to improve the power quality in grid-tied MG under DoS attack. It aims to regulate the compensating current of each MFGTI to cooperatively eliminate the harmonics and unbalanced current at the point of common coupling (PCC) of grid-tied MG. In addressing the aforementioned two challenges, the main contributions of this article are summarized as follows.

1) Unlike [5], [6], [7], [8], [9], [10], to address the first challenge mentioned before, the residual capacity of each MFGTI is adjusted by the active power factor in response to variations in accessible active power and harmonic and unbalanced current. The control method has the ability to adequately compensate for harmonics and unbalanced currents. Moreover, the power quality improvement and active power supply tasks can both be fairly shared among all MFGTIs without capacity waste.
2) Compared to [12], [13], [20], to address the second challenge mentioned before, the ETM is constructed to resist DoS attack and reduce communication burden simultaneously under a general DoS attack model with mild assumptions on attack frequency and duration. Moreover, the proposed ETM is executed under a selected

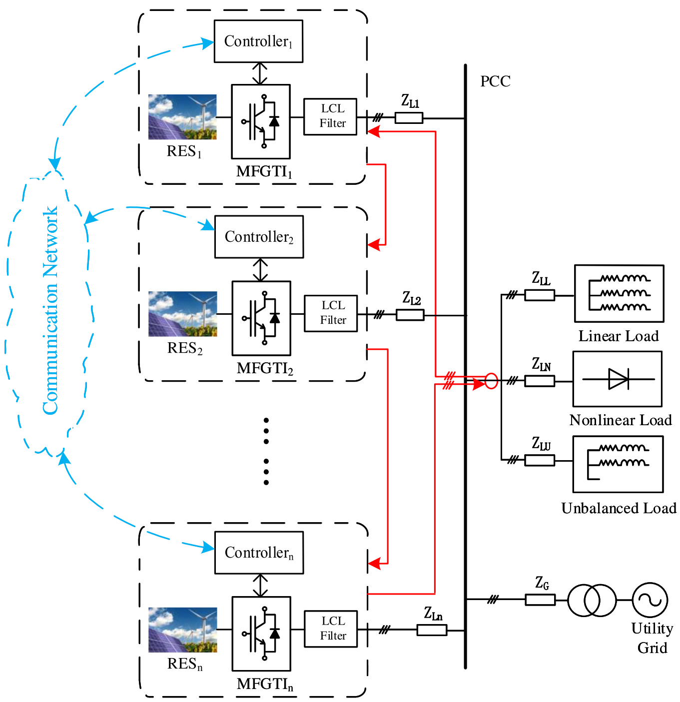

Fig. 1. Overview of the grid-tied MG architecture.

event-detection period while avoiding Zeno behavior. The proposed method achieves functional requirements 2) and 3) in the second challenge.

3) To fulfill functional requirements 1) and 4) in the second challenge, explicit mathematical formulations are provided for the convergence speed, accuracy, and the operating regions of parameters, all of which can be adjusted based on the desired control effectiveness and performance. Moreover, the operating regions reveal the relationship between triggering frequency, DoS attack tolerance, fluctuation ranges and stabilization time.

The rest of this article is organized as follows. Section II is the problem formulation. The main theoretical result is analyzed and provided in Section III. The simulation result is given in Section IV. Finally, Section V concludes this article.

II. Problem Formulation

A. MG Architecture

Consider the grid-tied MG depicted in Fig. 1, comprising multiple MFGTIs denoted as MFGTI$_k$ ($k = 1, 2, \ldots, N$). Each MFGTI$_k$ serves as the interface for RESs, such as photovoltaics and wind turbines, connecting to the PCC through an LCL filter with line impedance Z_{Lk}. The MG is linked to the utility grid via a transformer. Due to the presence of nonlinear and unbalanced loads in the MG, the power quality at the PCC deteriorates because of abundant harmonics and unbalanced current caused by the loads. This further jeopardizes the stable and economic operation of the utility grid. To improve the power quality, the local Controller$_k$ is configured to regulate the compensating current of each MFGTI$_k$, utilizing a distributed control architecture.

The communication network, whose topology is described by an undirected connected graph $\mathcal{G} = (\mathcal{V}, \mathcal{E}, A)$, is introduced to realize the information transmission between neighboring MFGTIs in the distributed control architecture. The node set $\mathcal{V} = \{1, 2, \ldots, N\}$ contains all the MFGTIs, and the edge set $\mathcal{E} = \{(k, j)|k, j \in \mathcal{V}\}$ contains all the communication channels where $(k, j) \in \mathcal{E}$ if the information of MFGTI$_k$ and MFGTI$_j$ can be transmitted directly through the communication network. Define the neighboring set of MFGTI$_k$ as $N_k = \{j \in \mathcal{V}|(k, j) \in \mathcal{E}\}$ with the cardinal number $|N_k|$. The weight matrix $A = \{a_{kj}\} \in R^{N\times N}$ is defined as $a_{kj} = a_{jk} > 0$ if $(k, j) \in \mathcal{E}$, otherwise $a_{kj} = a_{jk} = 0$, and it is assumed $a_{kk} = 0$. The Laplacian matrix of $\mathcal{G}$ is $L = \{l_{kj}\} \in R^{N\times N}$ where $l_{kj} = -a_{kj}$ for $k \neq j$, and $l_{kk} = \sum_{j=1}^{N} a_{kj}$.

B. DoS Attack Description

The DoS attack interferes with the communication network to prevent information transmission among MFGTIs. It disrupts the power quality improvement task by compromising data availability in the distributed control architecture. Denote $\mathcal{A}_v = [h_v, h_v + \tau_v)$ as the vth DoS attack interval. Define the following attack and healthy intervals in $[\tau, t)$ as:

$$\mathcal{A}(\tau, t) = \cup_v \mathcal{A}_v \cap [\tau, t), \quad \mathcal{H}(\tau, t) = [\tau, t)\backslash\mathcal{A}(\tau, t)$$

where the symbol $\backslash$ denotes the relative complement. During $\mathcal{A}(\tau, t)$, all information transmissions between MFGTIs are blocked, while transmissions are enabled in $\mathcal{H}(\tau, t)$. Due to restrictions on resources and energy consumed by adversaries, the frequency and duration of a DoS attack are constrained as follows by a mild condition. Moreover, The considered DoS attack model is capable of capturing a wide range of scenarios, including periodic, stochastic, and protocol-aware jamming attacks [21].

Assumption 1: There exists positive constants η, κ, T_f, and T_d such that $n(\tau, t) \leq \eta + \frac{t-\tau}{T_f}$ and $|\mathcal{A}(\tau, t)| \leq \kappa + \frac{t-\tau}{T_d}$.

C. Control Purpose

The load current is transmitted to each MFGTI though the electric line, delineated as the red transmission path in Fig. 1, independent of the communication network. Subsequently, $i_{LC}(t)$ can be measured locally by the current sensor configured at each MFGTI. The capacity of MFGTI$_k$ is identified by I_k, which is divided into the $I_k^a(t)$ and $I_k^r(t)$ at time t according to $I_k = \sqrt{(I_k^a(t))^2 + (I_k^r(t))^2}$ as illustrated in [20], where $I_k^a(t)$ and $I_k^r(t)$ are positive. The active part $I_k^a(t)$ is related to the maximum active power output of MFGTI$_k$, and it is time-varying due to the stochastic characteristics of the accessible power from RES$_k$. On the other hand, the nonactive part $I_k^r(t)$ can be regarded as the residual capacity of MFGTI$_k$. The maximum compensation ability of MFGTI$_k$ is revealed by the residual capacity according to $|i_k^c(t)| \leq I_k^r(t)$. The following purpose is considered in the power quality improvement task.

Purpose 1: The harmonics and unbalanced current is fairly compensated by all MFGTIs, namely

$$\sum_k i_k^c + i_{LC} = 0 \tag{1}$$

$$\frac{i_k^c}{I_k^r} = \frac{i_j^c}{I_j^r} \quad (\forall k, j \in \mathcal{V}). \tag{2}$$

Purpose 1 is well-defined when the total residual capacity of all MFGTIs is sufficient to compensate the current i_{LC}.

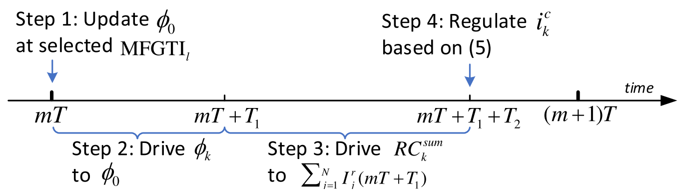

Fig. 2. Time chat of control flow.

However, this sufficiency is often compromised for the variations of accessible active power I_k^a and harmonic and unbalanced current i_{LC}. When the total residual capacity is insufficient, i.e., $|i_{LC}| > \sum_{k=1}^N I_k^r$, the current i_{LC} cannot be fully compensated since $I_k^r \geq |i_k^c|$. In this case, a portion of the harmonics and unbalanced current will inject into the PCC, further damaging the utility grid. To ensure sufficient residual capacity, each MFGTI_k regulates its own active current as $\phi_k(t)I_k^a(t)$ since $I_k^r(t) = \sqrt{I_k^2 - (\phi_k(t)I_k^a(t))^2}$, where the active power factor $\phi_k(t) \in [0, 1]$ is controlled to achieve the following control purpose.

Purpose 2: Each MFGTI provides the residual capacity fairly to compensate the harmonics and unbalanced current adequately, namely

$$|i_{LC}| \leq \sum_k I_k^r \tag{3}$$

$$\phi_k = \phi_j, \quad (\forall k, j \in \mathcal{V}). \tag{4}$$

Equation (2) implies that the power quality improvement task is proportionally shared among all MFGTIs based on their individual residual capacities. Moreover, (4) shows that the active current output ratio $\frac{\phi_k(t)I_k^a(t)}{I_k^a(t)}$ for each MFGTI_k achieves a unified value, ensuring fair distribution of the active power supply task among all MFGTIs. These purposes address the fair ancillary duty and utilization of MFGTIs.

The distributed resilient controller of each MFGTI will be designed to achieve Purposes 1 and 2 despite the harmful effects caused by a DoS attack. Meanwhile, the ETM is introduced to comprehensively determine the triggering time instants of each MFGTI, considering the occurrence of a DoS attack and communication resource limitations.

III. Resilient Event-Triggered Control of MFGTI Against DoS Attack

A. Control Flow

The control flow about MFGTIs in each time interval $[mT, (m+1)T)$ for $m = 0, 1, 2, \ldots$ is shown as follows, where the periods T_1 and T_2 will be calculated later and $T > T_1 + T_2$. The time chat is given in Fig. 2.

Control Flow

- *Step 1: Desired active power factor control*. The desired active power factor ϕ_0 is updated at time instant mT at the selected MFGTI_l.
- *Step 2: Individual residual capacity regulation*. The active power factor ϕ_k for each MFGTI_k is driven to the desired value ϕ_0 in time interval $[mT, mT + T_1)$.
- *Step 3: Total residual capacity estimation*. Each MFGTI_k updates its own estimated value of total residual capacity, i.e., $\mathrm{RC}_k^{\mathrm{sum}}$, in time interval $[mT + T_1, mT + T_1 + T_2)$, such that $\mathrm{RC}_k^{\mathrm{sum}}$ converges to $N \cdot I_k^r(mT + T_1)$.
- *Step 4: Compensating current reference regulation*. The compensating current reference of MFGTI_k is calculated as

$$i_k^c(t) = \begin{cases} -\frac{I_k^r(t)}{\mathrm{RC}_k^{\mathrm{sum}}(mT+T_1+T_2)} i_{LC}(t) \\ \quad \text{if } |i_{LC}(t)| \leq \mathrm{RC}_k^{\mathrm{sum}}(mT + T_1 + T_2) \\ -\mathrm{sign}(i_{LC}(t))I_k^r(t), \quad \text{otherwise} \end{cases} \tag{5}$$

where $t \in [mT + T_1 + T_2, (m+1)T + T_1 + T_2)$ and $\mathrm{sign}(\cdot)$ is the sign function.

Remark 1: The compensating current reference is provided by the proposed "Control Flow" and utilized by the inner control locally configured in MFGTI. The inner control regulates the actual compensating current of each MFGTI to track this reference, thereby compensating for the harmonics and unbalanced current at the PCC. It is reasonable to assume that this reference can be well-tracked by the inner control, whose detailed mechanism is omitted in this study and can be found in [20].

Section III-B–III-D will discuss the detailed control methods for Steps 1–3 under DoS attack, respectively, and these methods are compatible with distributed control architecture.

B. Desired Active Power Factor Control

The desired active power factor control in Step 1 of "Control Flow" is constructed as (6), where ϕ_0 is configured and updated at the selected MFGTI_l at each time instant mT

$$\phi_0((m+1)T) = \phi_0(mT) + K \cdot \mathrm{sign}_\varepsilon \left(\mathrm{RC}_l^{\mathrm{sum}}(mT) - \varepsilon - I_{\max}\right). \tag{6}$$

Noted that $I_{\max} = \max\{|i_{LC}(t)|, t \leq mT\}$, K and ε are positive constants, and the function $\mathrm{sign}_\varepsilon(x) = \mathrm{sign}(x)$ if $|x| \geq \varepsilon$ and $\mathrm{sign}_\varepsilon(x) = 0$ if $|x| < \varepsilon$.

At the time instant mT, MFGTI_l calculates the desired active power factor $\phi_0((m+1)T)$ based on (6). It can be observed from (6) that $\mathrm{RC}_l^{\mathrm{sum}}(mT) \leq I_{\max}$ leads to a decrease in ϕ_0. This implies that the active power output is guided to be reduced to provide more residual capacity for power quality improvement when the total residual capacity is insufficient. On the other hand, $\mathrm{RC}_l^{\mathrm{sum}}(mT) \geq I_{\max} + 2\varepsilon$ leads to an increase in ϕ_0, demonstrating that the active power output is guided to be increased to fully exploit the MGFTIs' power supply capacity when the total residual capacity is superabundant for power quality improvement. The positive parameter ε is introduced to prevent the chattering of ϕ_0. The adjustment of ϕ_0 in (6) reflects the ability to dynamically regulate MFGTI's residual capacity based on accessible active power and harmonic and unbalanced current, without incurring capacity waste.

Remark 2: The control law (6) is implemented at MFGTI_l locally, and the information transmission is not required. Its control performance does not depend on the communication network and is not influenced by DoS attack.

C. Individual Residual Capacity Regulation

To implement the regulation task mentioned in Step 2 of the "Control Flow," the distributed control method is constructed to drive ϕ_k of each MFGTI_k to the desired value ϕ_0. This desired value is located at MFGTI_l and can only be transmitted to the neighboring MFGTI_m for $m \in N_l$. Meanwhile, the ETM is introduced to reduce communication burden. Considering the time interval $[mT, mT+T_1)$, denote the triggering time instants corresponding to ϕ_k as $\{n_s^{\phi,k}T_e\}_{s=0}^{\infty}$, where the positive integers $\{n_s^{\phi,k}\}_{s=0}^{\infty}$ satisfy $n_0^{\phi,k} < n_1^{\phi,k} < \ldots < n_s^{\phi,k} < \ldots$, and the positive constant T_e is the event-detection period satisfying $T_e < T_1$. The factor ϕ_k is regulated as follows for $t \in [n_s^{\phi,k}T_e, n_{s+1}^{\phi,k}T_e)$:

$$\begin{aligned} \frac{d}{dt}\phi_k(t) &= K_1 u_k^{\phi}(t) \\ u_k^{\phi}(t) &= \sum_{j=1}^{N} a_{kj}\left(\phi_j(n_{s'(t)}^{\phi,j}T_e) - \phi_k(n_s^{\phi,k}T_e)\right) \\ &\quad + a_{k0}\left(\phi_0((m+1)T) - \phi_k(n_s^{\phi,k}T_e)\right) \end{aligned} \tag{7}$$

where $n_{s'(t)}^{\phi,j}T_e = \max\{n_s^{\phi,j}T_e | n_s^{\phi,j}T_e \le t\}$, the constant K_1 is positive, and $a_{k0} > 0$ if MFGTI_k can receive the information ϕ_0 through communication network directly, otherwise $a_{k0} = 0$. It is assumed that at least one of a_{k0} is positive for all k.

Each MFGTI_k broadcasts its own information $\phi_k(n_s^{\phi,k}T_e)$ to its neighbors at $n_s^{\phi,k}T_e$ under the control law (7). On the other hand, MFGTI_k receives the neighbors' triggered information $\phi_j(n_{s'(t)}^{\phi,j}T_e)$ for $j \in N_k$, which is stored and remained unchanged at MFGTI_k until the next triggered information is received from MFGTI_j. Less communication burden can be expected since only the discrete triggered information is used in (7).

The execution of distributed control law (7) requires the successful transmission of triggered information among MFGTIs, and it is threatened by DoS attack. The ETM should determine the triggering time instants considering the occurrence of DoS attack and limitation of communication resource synthetically. Denoting

$$e_k^{\phi}(t) = \phi_k(t) - \phi_k(n_s^{\phi,k}T_e)$$

for $t \in [n_s^{\phi,k}T_e, n_{s+1}^{\phi,k}T_e)$, and setting the parameter $\alpha^{\phi} \ge 0$, the ETM about ϕ_k under DoS attack is given in Algorithm 1, which is executed under the selected period T_e.

The dynamical scenario of Algorithm 1 is depicted as follows. Assuming the latest triggering time instant for ϕ_k is $n_s^{\phi,k}T_e$, MFGTI_k determines the next possible triggering time instant, denoted as $\widetilde{n}_{s+1}^{\phi,k}T_e$ here, by periodically checking the triggering condition $|e_k^{\phi}(nT_e)| > \alpha^{\phi}|u_k^{\phi}(nT_e)|$ with period T_e for each integer $n > n_s^{\phi,k}$. Although the triggering condition $|e_k^{\phi}(\widetilde{n}_{s+1}^{\phi,k}T_e)| > \alpha^{\phi}|u_k^{\phi}(\widetilde{n}_{s+1}^{\phi,k}T_e)|$ is satisfied, the information transmission at time instant $\widetilde{n}_{s+1}^{\phi,k}T_e$ may be prevented due to DoS attack. If $\widetilde{n}_{s+1}^{\phi,k}T_e \in \mathcal{A}(0,+\infty)$, MFGTI_k checks the existence of DoS attack from the time instant $\widetilde{n}_{s+1}^{\phi,k}T_e$ with the period T_e, and then the actual triggering time instant $n_{s+1}^{\phi,k}T_e$ is determined when it is confirmed that DoS attack is nonexistent. Note that $n_{s+1}^{\phi,k} > \widetilde{n}_{s+1}^{\phi,k}$ if DoS attack occurs at $\widetilde{n}_{s+1}^{\phi,k}T_e$; otherwise $n_{s+1}^{\phi,k} = \widetilde{n}_{s+1}^{\phi,k}$.

Remark 3: Algorithm 1 shows that $\{n_s^{\phi,k}T_e\}_{s=0}^{\infty}$ is contained in $\{nT_e\}_{n=0}^{\infty}$, and Zeno behavior can be avoided, i.e., an infinite number of communication rounds never be triggered within any finite temporal interval [15], since the interevent time intervals $(n_{s+1}^{\phi,k}T_e - n_s^{\phi,k}T_e)$ are strictly lower bounded by positive constant T_e. Mentioned that setting α^{ϕ} to 0 degenerates Algorithm 1 to the periodic transmission mechanism, and setting T_e close to 0 degenerates Algorithm 1 to the ETM based on continuous event checking. These observations highlight the superiority of the proposed ETM in Algorithm 1.

Algorithm 1: Event-Triggered Mechanism About ϕ_k Under DoS Attack.

- Initialize the parameters $n = n_s^{\phi,k}$ and $label_k^{\phi} = 0$;
- WHILE $n_{s+1}^{\phi,k}$ is not determined
  - IF $label_k^{\phi} == 0$ and $|e_k^{\phi}(nT_e)| > \alpha^{\phi}|u_k^{\phi}(nT_e)|$
    - ∗ IF DoS attack does NOT exists at time instant nT_e
      - · MFGTI_k determines $n_{s+1}^{\phi,k} = n$, transmits its own information $\phi_k(n_{s+1}^{\phi,k}T_e)$ to the neighbors, and sets $label_k^{\phi} = 0$;
    - ∗ END IF
    - ∗ IF DoS attack exists at time instant nT_e
      - · MFGTI_k sets $label_k^{\phi} = 1$;
    - ∗ END IF
  - END IF
  - IF $label_k^{\phi} == 1$
    - ∗ IF DoS attack does NOT exists at time instant nT_e
      - · MFGTI_k determines $n_{s+1}^{\phi,k} = n$, transmits its own information $\phi_k(n_{s+1}^{\phi,k}T_e)$ to the neighbors, and sets $label_k^{\phi} = 0$;
    - ∗ END IF
    - ∗ IF DoS attack exists at time instant nT_e
      - ·MFGTI_k sets $label_k^{\phi} = 1$;
    - ∗ END IF
  - END IF
  - Update $n := n + 1$;
- END WHILE

Theorem 1: If the following condition (8) is satisfied:

$$0 < C_1 < \frac{1}{2T_e}, \quad C_2 > 0, \quad C_3 > 0 \tag{8}$$

the distributed control law (7) with ETM Algorithm 1 yields (9) under DoS attack

$$|\phi_k(mT+T_1) - \phi_0((m+1)T)| \le \varepsilon_1 \tag{9}$$

where $C_1 = -K_1^2\overline{\lambda}_N^2 T_e\left(\frac{\alpha^{\phi}\overline{\lambda}_N}{1-\alpha^{\phi}\overline{\lambda}_N}\right)^2 - (K_1\overline{\lambda}_N + 2K_1^2\overline{\lambda}_N^2 T_e)\left(\frac{\alpha^{\phi}\overline{\lambda}_N}{1-\alpha^{\phi}\overline{\lambda}_N}\right) + (K_1\overline{\lambda}_1 - K_1^2\overline{\lambda}_N^2 T_e)$, $C_2 = \frac{2K_1\overline{\lambda}_N}{1-\alpha^{\phi}\overline{\lambda}_N}$, $C_3 = 2C_1 - \delta(2C_1 + C_2)$, $C_4 = (\kappa + 2T_e\eta)(2C_1 + C_2)$, $\delta = \frac{2T_e}{T_f} + \frac{1}{T_d}$, $\varepsilon_1 > 0$ can be arbitrarily small, and the period

$$T_1 \ge \frac{C_4}{C_3} - \frac{2}{C_3}\ln\frac{\varepsilon_1}{|\phi_k(mT) - \phi_0((m+1)T)|}.$$

Proof: See Appendix A. ■

D. Total Residual Capacity Estimation

The distributed control method designed to drive RC_k^{sum} toward $N \cdot I_k^r(mT+T_1)$ to achieve the estimation task outlined in Step 3 of "Control Flow." In addition, the ETM is introduced to reduce communication burden. During the time interval

Algorithm 2: Event-Triggered Mechanism About RC_k^{sum} Under DoS Attack.

- Replace the variables $n_s^{\phi,k}$, $n_{s+1}^{\phi,k}$, $label_k^{\phi}$, e_k^{ϕ}, α^{ϕ}, u_k^{ϕ}, and ϕ_k in Algorithm 1 into $n_s^{\mathrm{RC},k}$, $n_{s+1}^{\mathrm{RC},k}$, $label_k^{\mathrm{RC}}$, e_k^{RC}, α^{RC}, u_k^{RC}, and RC_k^{sum} respectively.

$[mT+T_1, mT+T_1+T_2)$, denote the triggering time instants corresponding to $\mathrm{RC}_k^{\mathrm{sum}}$ as $\{n_s^{\mathrm{RC},k}T_e\}_{s=0}^{\infty}$, where the positive integers $\{n_s^{\mathrm{RC},k}\}_{s=0}^{\infty}$ satisfy $n_0^{\mathrm{RC},k} < n_1^{\mathrm{RC},k} < \ldots < n_s^{\mathrm{RC},k} < \ldots$ and $T_e < T_2$. The estimated value $\mathrm{RC}_k^{\mathrm{sum}}$ is controlled as follows for $t \in [n_s^{\mathrm{RC},k}T_e, n_{s+1}^{\mathrm{RC},k}T_e)$:

$$\begin{aligned}\frac{d}{dt}\mathrm{RC}_k^{\mathrm{sum}}(t) &= K_2 u_k^{\mathrm{RC}}(t)\\ u_k^{\mathrm{RC}}(t) &= \sum_{j=1}^{N} a_{kj}\Big(\mathrm{RC}_j^{\mathrm{sum}}(n_{s'(t)}^{\mathrm{RC},j}T_e)\\ &\quad -\mathrm{RC}_k^{\mathrm{sum}}(n_s^{\mathrm{RC},k}T_e)\Big) \qquad (10)\end{aligned}$$

where $n_{s'(t)}^{\mathrm{RC},j}T_e = \max\{n_s^{\mathrm{RC},j}T_e | n_s^{\mathrm{RC},j}T_e \le t\}$ and the constant K_2 is positive. Denote

$$e_k^{\mathrm{RC}}(t) = \mathrm{RC}_k^{\mathrm{sum}}(t) - \mathrm{RC}_k^{\mathrm{sum}}(n_s^{\mathrm{RC},k}T_e)$$

for $t \in [n_s^{\mathrm{RC},k}T_e, n_{s+1}^{\mathrm{RC},k}T_e)$, and set the parameter $\alpha^{\mathrm{RC}} \ge 0$. Considering the occurrence of DoS attack and limitation of communication resource synthetically, the ETM about $\mathrm{RC}_k^{\mathrm{sum}}$ is provided in Algorithm 2. Given the significant similarities between Algorithms 1 and 2, and the space constraint, we provide a concise elucidation of Algorithm 2.

Theorem 2: Initialize the estimated total residual capacity as $\mathrm{RC}_k^{\mathrm{sum}}(mT+T_1) = N \cdot I_k^r(mT+T_1)$. If the following condition (11) is satisfied:

$$0 < \overline{C}_1 < \frac{1}{2T_e}, \quad \overline{C}_2 > 0, \quad \overline{C}_3 > 0 \qquad (11)$$

then the distributed control law (10) with ETM Algorithm 2 yields (12) under DoS attack

$$|\mathrm{RC}_k^{\mathrm{sum}}(mT+T_1+T_2) - \sum_{j=1}^{N} I_j^r(mT+T_1)| \le \varepsilon_2 \qquad (12)$$

where $\overline{C}_1 = -K_2^2\lambda_N^2T_e\left(\frac{\alpha^{\mathrm{RC}}\lambda_N}{1-\alpha^{\mathrm{RC}}\lambda_N}\right)^2 - (K_2\lambda_N + 2K_2^2\lambda_N^2T_e)\left(\frac{\alpha^{\mathrm{RC}}\lambda_N}{1-\alpha^{\mathrm{RC}}\lambda_N}\right) + (K_2\lambda_2 - K_2^2\lambda_N^2T_e)$, $\overline{C}_2 = \frac{2K_2\lambda_N}{1-\alpha^{\mathrm{RC}}\lambda_N}$, $\overline{C}_3 = 2\overline{C}_1 - \delta(2\overline{C}_1 + \overline{C}_2)$, $\overline{C}_4 = (\kappa + 2T_e\eta)(2\overline{C}_1 + \overline{C}_2)$, $\varepsilon_2 > 0$ can be arbitrarily small, and the period

$$T_2 \ge \frac{\overline{C}_4}{\overline{C}_3} - \frac{2}{\overline{C}_3}\ln\frac{\varepsilon_2}{|\mathrm{RC}_k^{\mathrm{sum}}(mT+T_1) - \sum_{j=1}^{N} I_j^r(mT+T_1)|}.$$

Proof: See Appendix B. ■

E. Main Result

Based on the above-mentioned discussion, the effectiveness of "Control Flow," which is composed of the regulation methods in Section III-B–III-D, is given in the following main result.

Theorem 3: The "Control Flow," which contains control laws (6), (7), (10), and ETMs Algorithms 1 and 2 under conditions (8) and (11), achieves Purposes 1 and 2 with acceptable fluctuation ranges under DoS attack, where the periods T_1 and T_2 are bounded in Theorem 1 and 2.

Proof: See Appendix C. ■

The typical dynamical scenario of "Control Flow" can be outlined as follows. Initially, harmonics and unbalanced current i_{LC} is adequately compensated by all MFGTIs in proportion. However, this ideal state may be disrupted due to fluctuations in i_{LC} and the accessible power from RESs. In response to this, the "Control Flow" is executed. In Step 1, the desired active power factor ϕ_0 is adjusted to reduce the difference between the total residual capacity and the maximum precompensated current. Step 2 aims to guide the individual active power factor ϕ_k of each MFGTI_k to the desired value ϕ_0, ensuring sufficient individual residual capacity and proportional sharing of the active power supply task. Subsequently, Step 3 estimates the new total residual capacity, used to regulate the proportional compensating current reference i_k^c in Step 4. With the proposed "Control Flow," executed in cycles of duration T, harmonics and unbalanced current i_{LC} is once again sufficiently and fairly compensated by all MFGTIs.

The parameter selection guidance of "Control Flow" is given as follows. With the inequality $C_2 > 0$, we get $\frac{\alpha^{\phi}\overline{\lambda}_N}{1-\alpha^{\phi}\overline{\lambda}_N} \ge 0$. Regarding C_1 as the quadratic function about the variable $\frac{\alpha^{\phi}\overline{\lambda}_N}{1-\alpha^{\phi}\overline{\lambda}_N}$, $C_1 > 0$ leads to

$$K_1T_e < \frac{\overline{\lambda}_1}{\overline{\lambda}_N^2} \qquad (13)$$

$$\frac{\alpha^{\phi}\overline{\lambda}_N}{1-\alpha^{\phi}\overline{\lambda}_N} \in [0, \omega_1) \qquad (14)$$

where $\omega_1 = \frac{\sqrt{\Delta_1}-1}{2K_1T_e\overline{\lambda}_N} - 1$ and $\Delta_1 = 4K_1T_e(\overline{\lambda}_1 + \overline{\lambda}_N) + 1$. Furthermore, under condition (13), $C_1 < \frac{1}{2T_e}$ leads to

$$\frac{\alpha^{\phi}\overline{\lambda}_N}{1-\alpha^{\phi}\overline{\lambda}_N} \in \begin{cases}[0, +\infty), & \text{if } \Delta_2 \le 0\\ [\omega_2, +\infty), & \text{if } \Delta_2 > 0\end{cases} \qquad (15)$$

where $\omega_2 = \max\{0, \frac{\sqrt{\Delta_2}-1}{2K_1T_e\overline{\lambda}_N} - 1\}$ and $\Delta_2 = 4K_1T_e(\overline{\lambda}_1 + \overline{\lambda}_N) - 1$. Combing (14) and (15) yields

$$\alpha^{\phi} \in \begin{cases}(0, \frac{\omega_1}{(1+\omega_1)\overline{\lambda}_N}), & \text{if } \Delta_2 \le 0\\ (\frac{\omega_2}{(1+\omega_2)\overline{\lambda}_N}, \frac{\omega_1}{(1+\omega_1)\overline{\lambda}_N}), & \text{if } \Delta_2 > 0.\end{cases} \qquad (16)$$

Similarly, condition (11) yields

$$K_2T_e < \frac{\lambda_2}{\lambda_N^2} \qquad (17)$$

$$\alpha^{\mathrm{RC}} \in \begin{cases}(0, \frac{\overline{\omega}_1}{(1+\overline{\omega}_1)\lambda_N}), & \text{if } \overline{\Delta}_2 \le 0\\ (\frac{\overline{\omega}_2}{(1+\overline{\omega}_2)\lambda_N}, \frac{\overline{\omega}_1}{(1+\overline{\omega}_1)\lambda_N}), & \text{if } \overline{\Delta}_2 > 0\end{cases} \qquad (18)$$

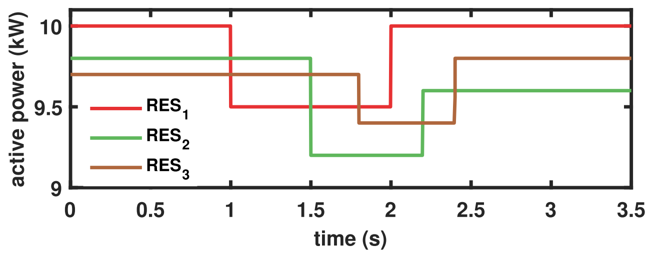

Fig. 3. Accessible active powers from RESs.

where $\overline{\omega}_1 = \frac{\sqrt{\overline{\Delta}_1}-1}{2K_2T_e\lambda_N} - 1, \overline{\omega}_2 = \max\{0, \frac{\sqrt{\overline{\Delta}_2}-1}{2K_2T_e\lambda_N} - 1\}, \overline{\Delta}_1 = 4K_2T_e(\lambda_2+\lambda_N)+1$, and $\overline{\Delta}_2 = 4K_2T_e(\lambda_2+\lambda_N)-1$. Conditions (13), (16), (17), and (18) ensure the operating regions of parameters K_1, K_2, α^{ϕ}, α^{RC}, and T_e. Under the determination of these parameters, $C_3 > 0$ and $\overline{C}_3 > 0$ lead to

$$\delta = \frac{2T_e}{T_f} + \frac{1}{T_d} < \min\left\{\frac{2C_1}{2C_1+C_2}, \frac{2\overline{C}_1}{2\overline{C}_1+\overline{C}_2}\right\} \tag{19}$$

which indicates the proposed "Control Flow's" tolerance of DoS attack.

Remark 4: The parameters α^{ϕ}, α^{RC}, and T_e are associated with triggering frequency, DoS attack tolerance, and stabilization time. Larger values of these parameters reduce the triggering frequency according to Algorithms 1 and 2. However, they decrease C_1, $\overline{C}_1$, C_3, and $\overline{C}_3$, and increase C_2 and $\overline{C}_2$. This implies that the proposed "Control Flow" becomes less tolerant to DoS attack and requires more time for stabilization. Conversely, smaller values of parameters α^{ϕ}, α^{RC}, and T_e have the opposite effects. This suggests that dense triggering is necessary to improve stabilization speed and resist serious DoS attack with long duration and high frequency. In practical applications, the selection of these parameters should consider the tradeoff between communication resource limitation, DoS attack tolerance level, and stabilization time requirement.

Remark 5: The fluctuation ranges ε_1 and ε_2, which can be selected arbitrarily small as given in Theorems 1 and 2, are acceptable in practical power quality improvement task of MG. Mentioned that smaller values of ε_1 and ε_2 lead to longer periods T_1 and T_2, and vice versa. The selection of their values depends on weighing between stabilization time and control precision.

IV. Simulation

A test system of grid-tied MG with three MFGTIs, whose architecture is given in Fig. 1, is constructed to verify the effectiveness of proposed control method through MATLAB/Simulink. The system voltage is three-phase, 220 V and 50 Hz. The impedance of transmission lines are $Z_{L1} = (0.02 + j2\times10^{-6})\Omega$, $Z_{L2} = (0.02 + j1\times10^{-6})\Omega$, $Z_{L3} = (0.03 + j4\times10^{-6})\Omega$, and $Z_{LL} = Z_{LN} = Z_{LU} = Z_G = (0.03 + j3\times10^{-6})\Omega$. The rated power of each MFGTI is 10 kVA. The accessible active powers from the three RESs are shown in Fig. 3 with the feature of low-frequency variation, since the fluctuation of RES needs a longer time scale than the dynamic control behavior of MFGTI. The node and edge sets in communication network are set as $\mathcal{V} = \{1,2,3\}$ and $\mathcal{E} = \{(1,2),(2,3)\}$, respectively.

Initially, the proposed control method for power quality improvement is not executed before time instant 0.5 s. The harmonics and unbalanced current caused by nonlinear and unbalanced loads is injected totally into the PCC of MG, as shown in Fig. 4.

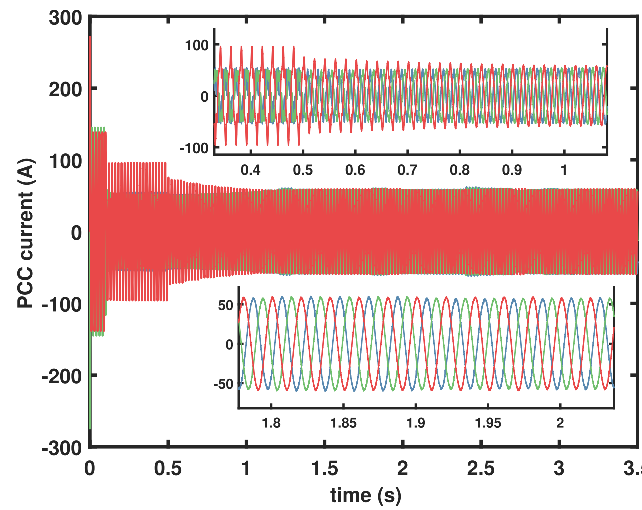

Fig. 4. PCC current of proposed "Control Flow" under mild DoS attack.

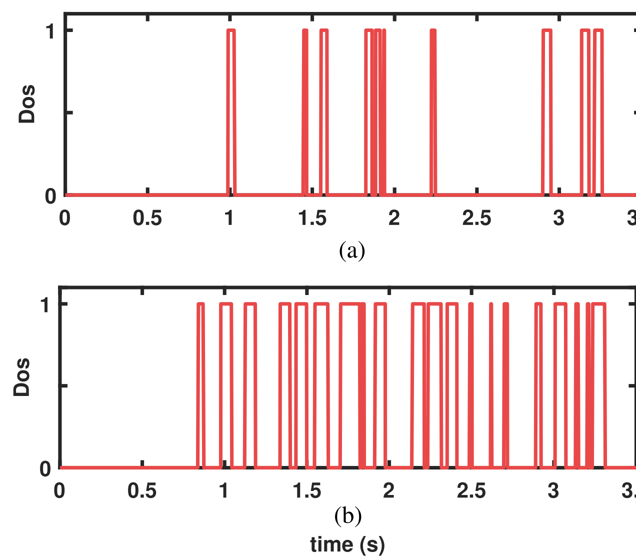

Fig. 5. (a) Mild DoS attack mode with average duty cycle 12%. (b) Severe DoS attack mode with average duty cycle 31%.

The total rated-current distortion (TRD) of PCC is increased above 40%, as illustrated in Fig. 6(a), which is much larger than 5% and does not met the requirement of standard [26]. At time instant 0.5 s, the proposed "Control Flow" is executed to improve power quality.

A. System Response Under Control Flow

The DoS attack signal and its dwell time in this case are shown in Fig. 5(a), where the occurrence of DoS attack corresponds to the value 1 at ordinate, otherwise the value is 0. The average duty cycle of DoS attack is 12%. The parameters in "Control Flow" are set as $K = 0.02$, $K_1 = 70$, $K_2 = 60$, $\alpha^{\phi} = 0.2$, and $\alpha^{\mathrm{RC}} = 0.05$. The periods are selected as $T_e = 0.001$ s, $T_1 = 0.07$ s, $T_2 = 0.02$ s, and $T = 0.1$ s. The desired active power factor is configured and updated at MFGTI_1.

In the time interval [0.5, 1) s, the accessible active power I_k^a from RES is close to the rated power of MFGTI 10 kVA, which makes the residual capacity insufficient for power quality improvement. Under the actions of Steps 1 and 2 in the proposed

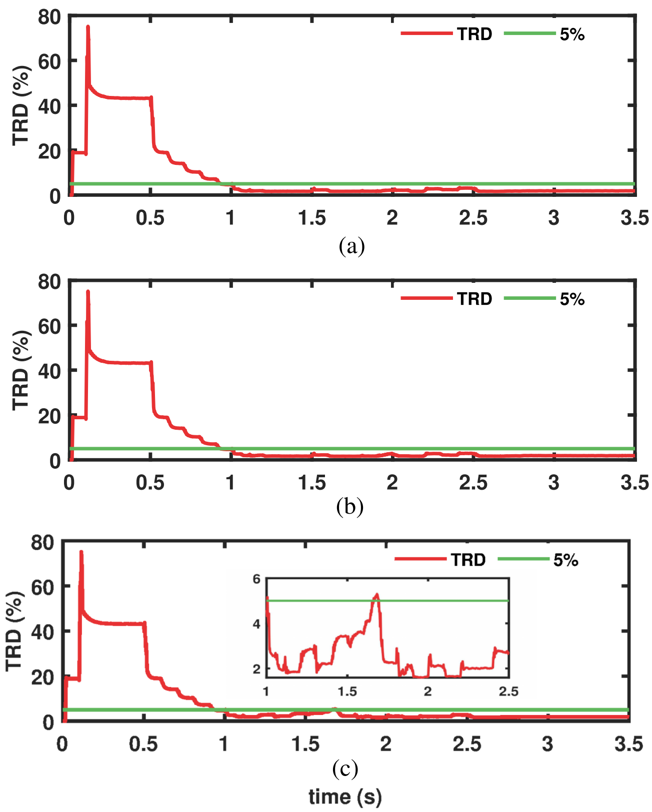

Fig. 6. TRD of PCC under (a) proposed "Control Flow" under mild DoS attack, (b) proposed "Control Flow" under severe DoS attack, (c) "Control Flow" with T-ETM.

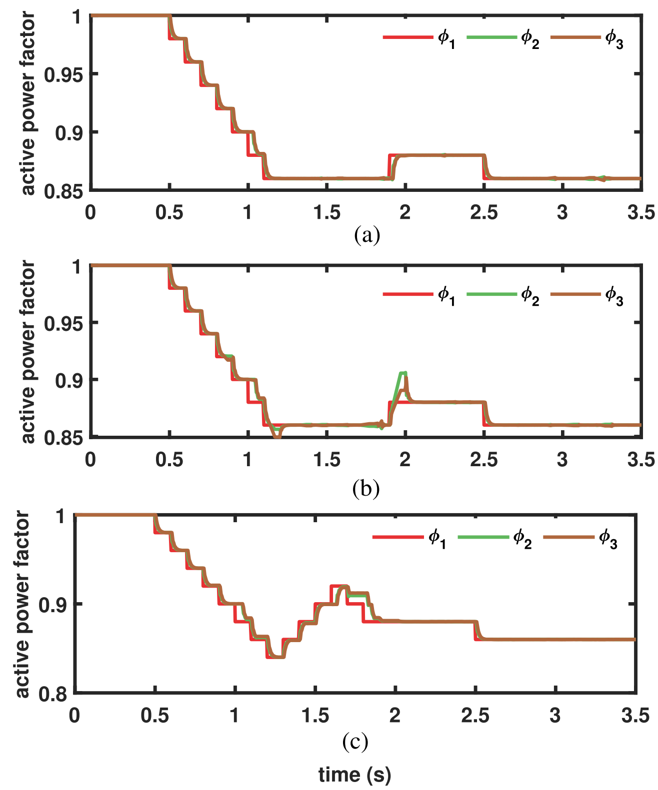

Fig. 7. Active power factors under (a) proposed "Control Flow" under mild DoS attack, (b) proposed "Control Flow" under severe DoS attack, (c) "Control Flow" with T-ETM.

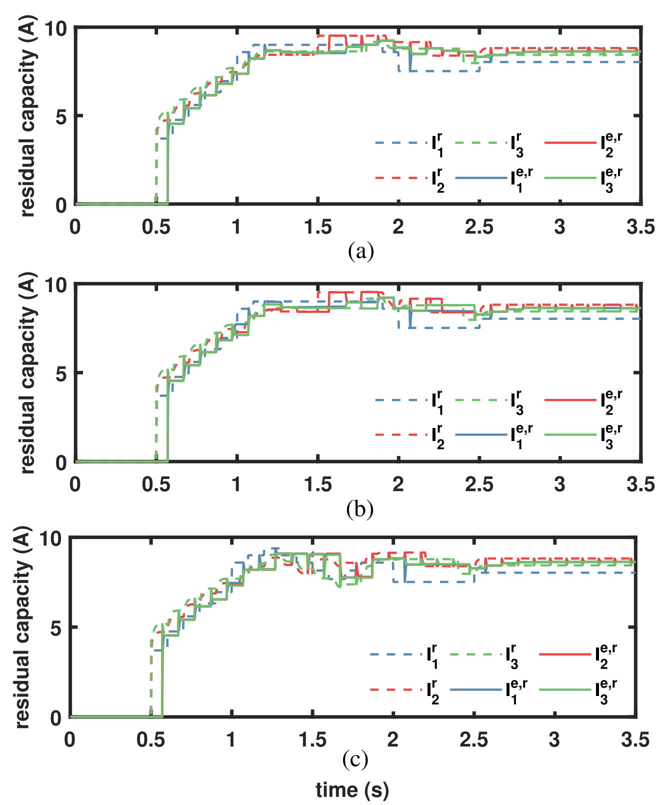

Fig. 8. Real and estimated residual capacity of each MFGTI under (a) proposed "Control Flow" under mild DoS attack, (b) proposed "Control Flow" under severe DoS attack, (c) "Control Flow" with T-ETM.

"Control Flow," the individual active power factor ϕ_k of each MFGTI is decreased to generate more residual capacity I_k^r until the total residual capacity is sufficient for compensating, as shown in Fig. 7(a). The consensus of active power factors illustrates the fair sharing of active power supply task among all MFGTIs. These results verify the achievement of Purpose 2.

In Fig. 8(a), the real residual capacity I_k^r of each MFGTI is increased with period T under the action of active power factor ϕ_k. Moreover, the estimated residual capacity at each MFGTI$_k$, which is defined as $I_k^{e,r}(t) = \frac{\mathrm{RC}_k^{\mathrm{sum}}(t)}{N}$, converges to the average value of total residual capacity in each period T. Furthermore, the difference between real and estimated total residual capacity, i.e., $(\sum_k I_k^r - \mathrm{RC}_k^{\mathrm{sum}})$, converges to 0 as given in Fig. 9(a). The above-mentioned results verify the effectiveness of estimation in Step 3 of "Control Flow." The evolution of sharing ratio $\mathrm{ratio}_k(t) = \frac{i_k^c(t)}{i_{LC}(t)}$ for each MFGTI$_k$ is given in Fig. 10(a), which demonstrates that the MFGTI with larger residual capacity provides more compensating current. In addition, Figs. 8(a) and 10(a) imply the achievement of control purpose (2). Defining $\mathrm{ratio}_{\sum}(t) = \sum_k \mathrm{ratio}_k(t) = \frac{\sum_k i_k^c(t)}{i_{LC}(t)}$, we multiply it by 0.25 in Fig. 10(a) to make the figure more compact. The harmonics and unbalanced current can be fully compensated since $\mathrm{ratio}_{\sum}$ converges to 1, and this result is also represented in Fig. 4. Moreover, the TRD of PCC is regulated below the standard value 5% in Fig. 6(a). According to the above-mentioned analysis, the achievement of Purpose 1 is verified.

In the time interval [1, 1.8) s, the accessible active power generated by RESs decreases, as illustrated in Fig. 3, resulting in

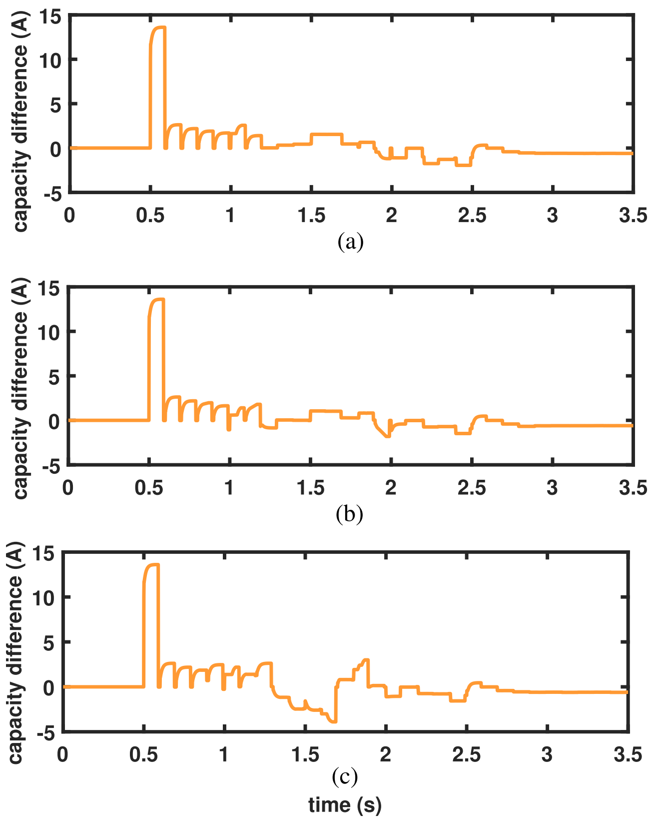

Fig. 9. Difference between real and estimated total residual capacity under (a) proposed "Control Flow" under mild DoS attack, (b) proposed "Control Flow" under severe DoS attack, (c) "Control Flow" with T-ETM.

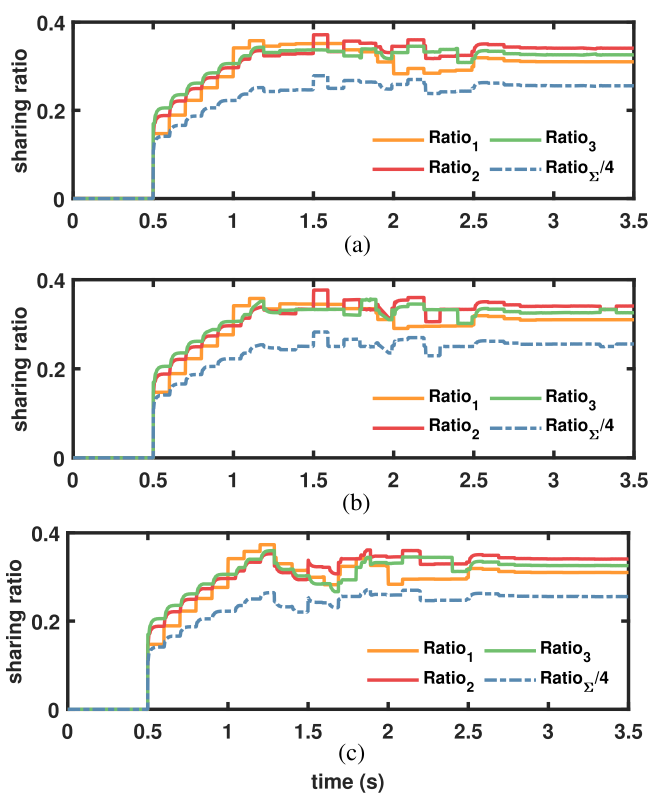

Fig. 10. Ratio$_k$ of each MFGTI under (a) proposed "Control Flow" under mild DoS attack, (b) proposed "Control Flow" under severe DoS attack, (c) "Control Flow" with T-ETM.

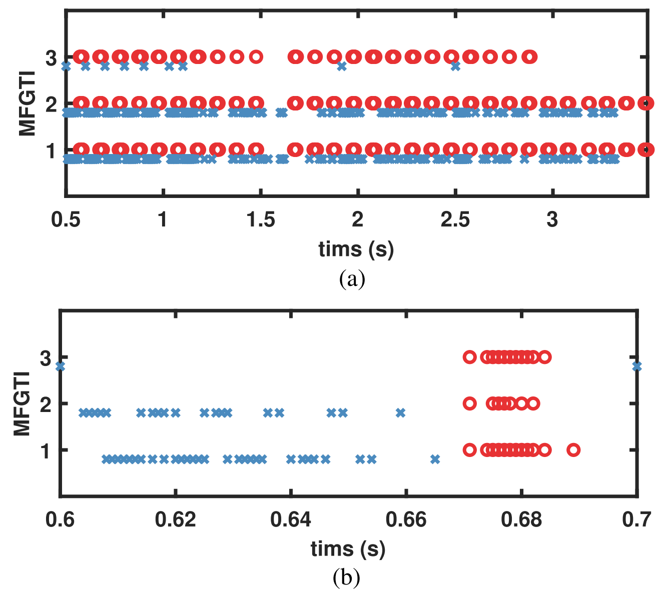

Fig. 11. Triggering time instants of proposed "Control Flow" under mild DoS attack in (a) whole action time interval [0.5, 3.5) s and (b) one cycle [0.6, 0.7) s.

an excess of total residual capacity. To fully utilize the available active power from RESs, the "Control Flow" increases the active power factor ϕ_k for each MFGTI$_k$, as depicted in Fig. 7(a). Subsequently, at time 2.5 s, the "Control Flow" decreases the active power factor ϕ_k in response to an increase in accessible active power during the interval [2, 2.5) s to provide sufficient residual capacity. Referring to Figs. 6(a)–10(a), it is evident that both Purposes 1 and 2 can still be achieved in these scenarios despite fluctuations in accessible active power, as previously analyzed.

B. Comparison Under Different DoS Attack

Figs. 6(b)–10(b) illustrate the system response under a more severe DoS attack scenario presented in Fig. 5(b), with a DoS average duty cycle of 31%. In contrast to the system response under mild DoS attack, as discussed in Section IV-A, a more severe attack induces additional fluctuations in system dynamics. Specifically, during the time interval $[1.9, 2]$ s, both Figs. 7(b) and 9(b) exhibit fluctuations in the active power factor and the difference between real and estimated total residual capacity. These fluctuations arise from the impact of the DoS attack, leading to reduced control performance at specific instants under severe DoS conditions. Nevertheless, regardless of the severity of the DoS attack, the adverse effects generated by the attack are promptly counteracted by the proposed "Control Flow," as illustrated in Figs. 6(b)–10(b). Importantly, this resilience is achieved without compromising the successful realization of Purposes 1 and 2.

C. Effectiveness in Reducing Communication Burden

Fig. 11 gives the triggering time sequence of all MFGTIs under DoS attack in the whole action time interval and one cycle of "Control Flow," respectively. The cases about active power factor ϕ_k and estimated total residual capacity $\mathrm{RC}_k^{\mathrm{sum}}$ are both presented. The unequal triggering periods shown in these figures reveal the ability of ETM in adjusting communication frequency

TABLE I
COMPARISON OF COMMUNICATION NUMBER BETWEEN ETM AND PSM

	MFGTI_1	MFGTI_2	MFGTI_3
ETM about ϕ_k	9	252	339
PSM about ϕ_k	27	2700	2700
rate about ϕ_k	33.3%	9.3%	12.6%
ETM about $\mathrm{RC}_k^{\mathrm{sum}}$	166	242	247
PSM about $\mathrm{RC}_k^{\mathrm{sum}}$	2700	2700	2700
rate about $\mathrm{RC}_k^{\mathrm{sum}}$	6.1%	8.9%	9.1%

based on the system's state. Since the desired active power factor ϕ_0 is configured at MFGTI_1, the event about ϕ_1 is only triggered when ϕ_0 changes, and this makes the triggering number of ϕ_1 much less than those of ϕ_2 and ϕ_3. Table I summaries the communication number of Algorithms 1 and 2 under DoS attack. For comparison, the result under periodic sampling mechanism (PSM) with the period T_e, which is obtained by setting the parameters α^{ϕ} and α^{RC} as 0, is also given in Table I. It can be seen that the communication burden is reduced sharply under ETM compared with periodic sampling one.

D. Effectiveness in Resisting DoS Attack

To demonstrate the resilience of our proposed "Control Flow" against DoS attack, we replaced Algorithms 1 and 2 in the "Control Flow" with the traditional event-triggered mechanism (T-ETM), which is constructed without considering the occurrence of DoS attack. Taking ϕ_k as an example, a brief description of T-ETM is as follows. For MFGTI_k, suppose the last triggering time instant about ϕ_k is $n_s^{\phi,k}T_e$. If the condition $|e_k^{\phi}(nT_e)| > \alpha^{\phi}|u_k^{\phi}(nT_e)|$ is satisfied at some certain time instant $nT_e(n > n_s^{\phi,k})$, MFGTI_k determines the new triggering time instant $n_{s+1}^{\phi,k}T_e$ as nT_e, and broadcasts its own information $\phi_k(n_{s+1}^{\phi,k}T_e)$ to the neighbors consistently regardless of the presence of DoS attack at time nT_e.

Figs. 6(c)–10(c) illustrate the system response under the "Control Flow" with T-ETM. Notably, during the time interval $[1.1, 2]$ s, substantial fluctuations occur in the active power factor, ratio, the difference between real and estimated residual capacity, and TRD. Compared to Figs. 6(b)–10(b), the "Control Flow" with T-ETM fails to promptly mitigate the adverse effects of DoS attack. Furthermore, Fig. 6(c) indicates that TRD even exceeds the standard value, i.e., 5%. Contrasting Figs. 6(b)–10(b) and Figs. 6(c)–10(c), respectively, it is evident that "Control Flow" with T-ETM cannot achieve Purposes 1 and 2 under DoS attack in the case of accessible active power fluctuation. This underscores the superiority of our proposed "Control Flow" in resisting DoS attack.

V. CONCLUSION

This article explores distributed resilient event-triggered control method for MFGTIs in grid-tied MG under DoS attack, which ensures adequate compensation of harmonics and unbalanced current at the PCC under varying accessible active power from RES and the fair utilization among all MFGTIs. The mentioned specific functional requirements associated with power quality event-triggered control under DoS attack are all satisfied. Simulation results validate the effectiveness of the proposed approach. Future research will extend the control methodology to address different types of cyberattacks, such as replay attack and false data injection attack.

APPENDIX A
PROOF OF THEOREM 1

Denote the vectors $\varphi(t) = (\varphi_1(t), \ldots, \varphi_N(t))^T$ and $\hat{\varphi}(t) = (\hat{\varphi}_1(t), \ldots, \hat{\varphi}_N(t))^T$ where $\varphi_k(t) = \phi_k(t) - \phi_0((m+1)T)$ and $\hat{\varphi}_k(t) = \phi_k(n_{s'(t)}^{\phi,k}T_e) - \phi_0((m+1)T)$. Construct the candidate Lyapunov function $V(t) = \frac{1}{2}\varphi^T(t)\varphi(t)$, and rewrite the closed-loop system (7) into (20) for $t \in [nT_e, (n+1)T_e)$

$$\frac{d}{dt}\varphi(t) = -K_1\overline{L}\hat{\varphi}(nT_e). \tag{20}$$

Considering the interval $\mathcal{A}_v = [h_v, h_v + \tau_v)$, denote $\underline{n}_v = \max\{n|nT_e \le h_v\}$ and $\overline{n}_v = \min\{n|nT_e \ge h_v + \tau_v\}$, and construct the interval $\overline{\mathcal{A}}_v = [\underline{n}_vT_e, \overline{n}_vT_e)$, $\overline{\mathcal{A}}(\tau, t) = \bigcup_v \overline{\mathcal{A}}_v \cap [\tau, t)$, and $\overline{\mathcal{H}}(\tau, t) = [\tau, t)\backslash\overline{\mathcal{A}}(\tau, t)$. Furthermore, construct the intervals $\widetilde{\mathcal{A}}_w = [\underline{\xi}_wT_e, \overline{\xi}_wT_e)$ and $\widetilde{\mathcal{H}}_w = [\overline{\xi}_wT_e, \underline{\xi}_{w+1}T_e)$ such that $\bigcup_w \widetilde{\mathcal{A}}_w = \bigcup_v \overline{\mathcal{A}}_v$, where $\underline{\xi}_w$ and $\overline{\xi}_w$ are nonnegative integers satisfying $\underline{\xi}_w < \overline{\xi}_w < \underline{\xi}_{w+1}$. Obviously, we have $\overline{\mathcal{A}}(\tau, t) = \bigcup_w \widetilde{\mathcal{A}}_w \cap [\tau, t)$ and $\overline{\mathcal{H}}(\tau, t) = \bigcup_w \widetilde{\mathcal{H}}_w \cap [\tau, t)$.

Case 1: If $t \in \widetilde{\mathcal{H}}_w \cap [nT_e, (n+1)T_e)$, Algorithm 1 leads to $|e_k^{\phi}(nT_e)| \le \alpha^{\phi}|u_k^{\phi}(nT_e)|$. Denoting the vector $e^{\phi}(t) = (e_1^{\phi}(t), \ldots, e_N^{\phi}(t))^T$ yields $\| e^{\phi}(nT_e) \| \le \alpha^{\phi} \| \overline{L}\hat{\varphi}(nT_e) \| \le \alpha^{\phi}\overline{\lambda}_N \| \varphi(nT_e) - e^{\phi}(nT_e) \|$, which further gets

$$\| e^{\phi}(nT_e) \| \le \frac{\alpha^{\phi}\overline{\lambda}_N}{1 - \alpha^{\phi}\overline{\lambda}_N} \| \varphi(nT_e) \| . \tag{21}$$

According to (20), we have

$$\frac{d}{dt}\varphi(t) = -K_1\overline{L}(\varphi(nT_e) - e^{\phi}(nT_e)) \tag{22}$$

$$\varphi(t) = \varphi(nT_e) - (t - nT_e)K_1\overline{L}(\varphi(nT_e) - e^{\phi}(nT_e)). \tag{23}$$

Equations (21)–(23) get that

$$\begin{aligned} \frac{d}{dt}V(t) \le\ & K_1^2T_e\overline{\lambda}_N^2 \| \varphi(nT_e) - e^{\phi}(nT_e) \|^2 - K_1\overline{\lambda}_1||\varphi(nT_e)||^2 \\ & + K_1\overline{\lambda}_N \| \varphi(nT_e) \| \cdot \| e^{\phi}(nT_e) \| \\ =\ & -2C_1V(nT_e). \end{aligned} \tag{24}$$

Since $(t - nT_e)\varphi'(t) = \int_{nT_e}^{t} \varphi'(s)ds = \varphi(t) - \varphi(nT_e)$, it gets

$$\begin{aligned} V(nT_e) &= \frac{1}{2} \| \varphi(t) - (t - nT_e)\varphi'(t) \|^2 \\ &\ge V(t) - (t - nT_e)\frac{d}{dt}V(t). \end{aligned} \tag{25}$$

Under condition (8), substituting (25) into (24) gets $\frac{d}{dt}V(t) \le -\frac{2C_1}{1-2C_1(t-nT_e)}V(t) \le -2C_1V(t)$. This means that $V(t) \le e^{-2C_1(t-nT_e)}V(nT_e)$, which further implies

$$V(t) \le e^{-2C_1(t-\overline{\xi}_wT_e)}V(\overline{\xi}_wT_e), \quad t \in \widetilde{\mathcal{H}}_w. \tag{26}$$

Case 2: If $t \in \widetilde{\mathcal{A}}_w \cap [nT_e, (n+1)T_e)$, according to Algorithm 1 and (20), we have

$$\begin{aligned} \frac{d}{dt}V(t) &= (-K_1\overline{L}\hat{\varphi}(nT_e))^T\varphi(t) = (-K_1\overline{L}\hat{\varphi}(\underline{\xi}_wT_e))^T\varphi(t) \\ &\le K_1\overline{\lambda}_N \| \hat{\varphi}(\underline{\xi}_wT_e) \| \cdot \| \varphi(t) \| . \end{aligned} \tag{27}$$

Since $\underline{\xi}_w T_e \in \mathcal{H}(0,+\infty)$, it gets from Algorithm 1 that

$$\| \varphi(\underline{\xi}_w T_e) - \hat{\varphi}(\underline{\xi}_w T_e) \| = \| e^{\phi}(\underline{\xi}_w T_e) \| \leq \alpha^{\phi}\overline{\lambda}_N \| \hat{\varphi}(\underline{\xi}_w T_e) \|. \quad (28)$$

Combing (27) and (28) yields

$$\frac{d}{dt}V(t) \leq \frac{K_1\overline{\lambda}_N}{1-\alpha^{\phi}\overline{\lambda}_N} \| \varphi(\underline{\xi}_w T_e) \| \cdot \| \varphi(t) \|. \quad (29)$$

a) If $\| \varphi(t) \| \leq \| \varphi(\underline{\xi}_w T_e) \|$, we have $\frac{d}{dt}V(t) \leq \frac{K_1\overline{\lambda}_N}{1-\alpha^{\phi}\overline{\lambda}_N} \| \varphi(\underline{\xi}_w T_e) \|^2 = \frac{2K_1\overline{\lambda}_N}{1-\alpha^{\phi}\overline{\lambda}_N} V(\underline{\xi}_w T_e)$ based on (29). This implies

$$V(t) \leq \left((t-\underline{\xi}_w T_e)\frac{2K_1\overline{\lambda}_N}{1-\alpha^{\phi}\overline{\lambda}_N} + 1 \right) V(\underline{\xi}_w T_e). \quad (30)$$

b) If $\| \varphi(t) \| > \| \varphi(\underline{\xi}_w T_e) \|$, we have $\frac{d}{dt}V(t) \leq \frac{K_1\overline{\lambda}_N}{1-\alpha^{\phi}\overline{\lambda}_N} \| \varphi(t) \|^2 = \frac{2K_1\overline{\lambda}_N}{1-\alpha^{\phi}\overline{\lambda}_N} V(t)$ based on (29). This implies

$$V(t) \leq e^{(t-\underline{\xi}_w T_e)\frac{2K_1\overline{\lambda}_N}{1-\alpha^{\phi}\overline{\lambda}_N}} V(\underline{\xi}_w T_e). \quad (31)$$

Since $(t-\underline{\xi}_w T_e)\frac{2K_1\overline{\lambda}_N}{1-\alpha^{\phi}\overline{\lambda}_N} > 0$, integrating (30) and (31) yields

$$V(t) \leq e^{C_2(t-\underline{\xi}_w T_e)} V(\underline{\xi}_w T_e), \quad t \in \widetilde{\mathcal{A}}_w. \quad (32)$$

Combining (26) and (32) gets (33) for $t \in [mT, mT+T_1)$

$$V(t) \leq e^{-2C_1|\overline{\mathcal{H}}(mT,t)|+C_2|\overline{\mathcal{A}}(mT,t)|} V(mT). \quad (33)$$

Under Assumption 1, we have

$$\begin{aligned} |\overline{\mathcal{A}}(mT,t)| &\leq \kappa + \frac{t-mT}{T_d} + 2n(mT,t)T_e \\ &\leq \kappa + 2T_e\eta + \delta(t-mT) \end{aligned} \quad (34)$$

$$|\overline{\mathcal{H}}(mT,t)| = t - mT - |\overline{\mathcal{A}}(mT,t)|. \quad (35)$$

Substituting (34) and (35) into (33) gets $V(t) \leq e^{C_4-C_3(t-mT)}V(mT)$, which further leads to $\| \phi_k(t) - \phi_0((m+1)T) \|^2 \leq e^{C_4-C_3(t-mT)} \| \phi_k(mT) - \phi_0((m+1)T) \|^2$ for $t \in [mT, mT+T_1)$ and concludes the proof.

Appendix B
Proof of Theorem 2

Denoting the vectors $x(t) = (\mathrm{RC}_1^{\mathrm{sum}}(t), \ldots, \mathrm{RC}_N^{\mathrm{sum}}(t))^T$ and $\hat{x}(t) = (\hat{x}_1(t), \ldots, \hat{x}_N(t))^T$ where $\hat{x}_k(t) = \mathrm{RC}_k^{\mathrm{sum}}(n_{s'(t)}^{\mathrm{RC},k}T_e)$, the closed-loop system (10) can be written as $\frac{d}{dt}x(t) = -K_2L\hat{x}(t)$. Defining $\bar{x}(t) = \frac{1}{N}\mathbf{1}^T x(t) = \frac{1}{N}\sum_{j=1}^N x_j(t)$, it leads to

$$\frac{d}{dt}\bar{x}(t) = \frac{1}{N}(\mathbf{1}^T\frac{d}{dt}x(t)) = -\frac{K_2}{N}\mathbf{1}^T L\hat{x}(t) = 0 \quad (36)$$

where $\mathbf{1}$ denotes the N-dimensional column vector with all entries equal to one. Equation (36) implies $\bar{x}(t) \equiv \bar{x}(mT+T_1)$ for $t \in [mT+T_1, mT+T_1+T_2)$. Denoting the vectors $\tilde{x}(t) = x(t) - \bar{x}(mT+T_1)\mathbf{1}$ and $\hat{\tilde{x}}(t) = \hat{x}(t) - \bar{x}(mT+T_1)\mathbf{1}$, the closed-loop system (10) can be written as (37) for $t \in [nT_e, (n+1)T_e)$

$$\frac{d}{dt}\tilde{x}(t) = -K_2L\hat{\tilde{x}}(nT_e). \quad (37)$$

Constructing the candidate Lyapunov function $\tilde{V}(t) = \frac{1}{2}(\tilde{x}(t))^T\tilde{x}(t)$, the similar analysis in the proof of Theorem 1 yields $\| \mathrm{RC}_k^{\mathrm{sum}}(t) - \sum_{j=1}^N I_j^r(mT+T_1) \|^2 \leq e^{\overline{C}_4-\overline{C}_3(t-mT-T_1)} \cdot \| \mathrm{RC}_k^{\mathrm{sum}}(mT+T_1) - \sum_{j=1}^N I_j^r(mT+T_1) \|^2$ for $t \in [mT+T_1, mT+T_1+T_2)$, which further leads to (12).

Appendix C
Proof of Theorem 3

Consider the time interval $[mT+T_1+T_2, (m+1)T)$. If $|i_{LC}(t)| \leq \mathrm{RC}_k^{\mathrm{sum}}(mT+T_1+T_2)$ for some certain k, Theorem 2 ensures $|i_{LC}(t)| \leq \mathrm{RC}_j^{\mathrm{sum}}(mT+T_1+T_2)$ for all $j \in \mathcal{V}$, and then Step 4 in "Control Flow" yields

$$\begin{aligned} \frac{i_k^c(t)}{i_j^c(t)} &= \frac{I_k^r(t)}{I_j^r(t)} \cdot \frac{\mathrm{RC}_j^{\mathrm{sum}}(mT+T_1+T_2)}{\mathrm{RC}_k^{\mathrm{sum}}(mT+T_1+T_2)} \\ &= \frac{I_k^r(t)}{I_j^r(t)} \left(\frac{\varepsilon_2}{\mathrm{RC}_k^{\mathrm{sum}}(mT+T_1+T_2)} + 1 \right). \end{aligned} \quad (38)$$

If $|i_{LC}(t)| > \mathrm{RC}_k^{\mathrm{sum}}(mT+T_1+T_2)$ for some certain k, we have $|i_{LC}(t)| > \mathrm{RC}_j^{\mathrm{sum}}(mT+T_1+T_2)$ for all $j \in \mathcal{V}$, and then

$$\frac{i_k^c(t)}{i_j^c(t)} = \frac{\mathrm{sign}(i_{LC}(t))I_k^r(t)}{\mathrm{sign}(i_{LC}(t))I_j^r(t)} = \frac{I_k^r(t)}{I_j^r(t)}. \quad (39)$$

Moreover, Theorem 1 shows that $|\phi_k(t) - \phi_j(t)| \leq 2\varepsilon_1$. This together with (38) and (32) ensures control purposes (2) and (4) with acceptable fluctuation ranges since ε_1 and ε_2 can be selected small enough.

Control law (6) ensures $\phi_0((m+1)T)$ is decreased compared with $\phi_0(mT)$ when $\mathrm{RC}_l^{\mathrm{sum}}(mT) \leq I_{\max}$, which implies $\phi_k(t)$ of each MFGTI_k is decreased K units at $mT+T_1$ according to Theorem 1. This means $I_k^r(t)$ is increased since $I_k^r(t) = \sqrt{I_k^2 - (\phi_k(t)I_k^a(t))^2}$, and then we get $\mathrm{RC}_l^{\mathrm{sum}}$ is increased until $\mathrm{RC}_l^{\mathrm{sum}} > I_{\max} + 2\varepsilon$ based on (6). This ensures control purpose (3) when the parameter K is small enough. Under the case of sufficient total residual capacity, Step 4 in "Control Flow" ensures $\sum_j i_j^c(t) = -i_{LC}(t)\sum_j \frac{I_j^r(t)}{\mathrm{RC}_j^{\mathrm{sum}}(mT+T_1+T_2)}$ for $t \in [mT+T_1+T_2, (m+1)T)$, where $\sum_j \frac{I_j^r(t)}{\mathrm{RC}_j^{\mathrm{sum}}(mT+T_1+T_2)} \approx \frac{\sum_j I_j^r(t)}{\sum_j I_j^r(mT+T_1)}$ according to Theorem 2. Mentioned that the changing of $I_j^r(t)$ is only related to $I_j^a(t)$ in the time interval $[mT+T_1, (m+1)T)$ where $\phi_j(t)$ keeps constant. Due to the fact that the change of accessible power from RES_j is much slower than that of MFGTI_j's dynamical behavior [20], the active current $I_j^a(t)$ can be regarded as constant for $t \in [mT+T_1, (m+1)T)$, which further leads to $I_j^r(t) = I_j^r(mT+T_1)$. We then have $\sum_j \frac{I_j^r(t)}{\mathrm{RC}_j^{\mathrm{sum}}(mT+T_1+T_2)}$ is close to 1 and control purpose (1) can be achieved. Combining the above-mentioned analysis concludes the proof.

References

[1] S. Sen and V. Kumar, "Microgrid control: A comprehensive survey," *Annu. Rev. Control*, vol. 45, pp. 118–151, 2018.

[2] P. A. Karafotis, V. A. Evangelopoulos, and P. S. Georgilakis, "Evaluation of harmonic contribution to unbalance in power systems under non-stationary conditions using wavelet packet transform," *Electric Power Syst. Res.*, vol. 178, 2020, Art. no. 106026.

[3] J. Hu, Y. Shan, K. W. Cheng, and S. Islam, "Overview of power converter control in microgrids challenges, advances, and future trends," *IEEE Trans. Power Electron.*, vol. 37, no. 8, pp. 9907–9922, Aug. 2022.

[4] I. Khan, A. S. Vijay, and S. Doolla, "Nonlinear load harmonic mitigation strategies in microgrids: State of the art," *IEEE Syst. J.*, vol. 16, no. 3, pp. 4243–4255, Sep. 2022.

[5] L. Meng et al., "Distributed voltage unbalance compensation in islanded microgrids by using a dynamic consensus algorithm," *IEEE Trans. Power Electron.*, vol. 31, no. 1, pp. 827–838, Jan. 2016.

[6] J. Zhou, S. Kim, H. Zhang, Q. Sun, and R. Han, "Notice of Removal: Consensus-based distributed control for accurate reactive, harmonic, and imbalance power sharing in microgrids," *IEEE Trans. Smart Grid*, vol. 9, no. 4, pp. 2453–2467, Jul. 2018.

[7] A. Das, A. Shukla, A. B. Shyam, S. Anand, J. M. Guerreo, and S. R. Sahoo, "A distributed-controlled harmonic virtual impedance loop for AC microgrids," *IEEE Trans. Ind. Electron.*, vol. 68, no. 5, pp. 3949–3961, May 2021.

[8] L. S. Xavier, A. F. Cupertino, H. A. Pereira, and V. F. Mendes, "Partial harmonic current compensation for multifunctional photovoltaic inverters," *IEEE Trans. Power Electron.*, vol. 34, no. 12, pp. 11868–11879, Dec. 2019.

[9] R. Chilipi, A. Al Sumaiti, and B. Singh, "Control of grid-tied multiple distributed generation systems with cooperative compensation capabilities," *IEEE J. Emerg. Sel. Topics Ind. Electron.*, vol. 3, no. 3, pp. 821–833, Jul. 2022.

[10] W. Guo and W. Xu, "Research on optimization strategy of harmonic suppression and reactive power compensation of photovoltaic multifunctional grid connected inverter," *Int. J. Elect. Power Energy Syst.*, vol. 145, 2023, Art. no. 108649.

[11] X.-M. Zhang and Q.-L. Han, "Network-based H∞ filtering using a logic jumping-like trigger," *Automatica*, vol. 49, no. 5, pp. 1428–1435, 2013.

[12] J. Lu, M. Zhao, S. Golestan, T. Dragicevic, X. Pan, and J. M. Guerrero, "Distributed event-triggered control for reactive, unbalanced, and harmonic power sharing in islanded AC microgrids," *IEEE Trans. Ind. Electron.*, vol. 69, no. 2, pp. 1548–1560, Feb. 2022.

[13] J. Lu, X. Liu, M. Savaghebi, X. Hou, and P. Wang, "Distributed event-triggered control for harmonic voltage compensation in islanded AC microgrids," *IEEE Trans. Smart Grid*, vol. 13, no. 6, pp. 4190–4201, Nov. 2022.

[14] A. I. Rikos and C. N. Hadjicostis, "Event-triggered quantized average consensus via ratios of accumulated values," *IEEE Trans. Autom. Control*, vol. 66, no. 3, pp. 1293–1300, Mar. 2021.

[15] N. Lin and Q. Ling, "Dynamic periodic event-triggered consensus protocols for linear multiagent systems with network delay," *IEEE Syst. J.*, vol. 17, no. 1, pp. 1204–1215, Mar. 2023.

[16] J. Peng, B. Fan, Q. Yang, and W. Liu, "Distributed event-triggered control of DC microgrids," *IEEE Syst. J.*, vol. 15, no. 2, pp. 2504–2514, Jun. 2021.

[17] H. S. Sánchez, D. Rotondo, T. Escobet, V. Puig, and J. Quevedo, "Bibliographical review on cyber attacks from a control oriented perspective," *Annu. Rev. Control*, vol. 48, pp. 103–128, 2019.

[18] N. Zhao, P. Shi, W. Xing, and R. K. Agarwal, "Resilient event-triggered control for networked cascade control systems under denial-of-service attacks and actuator saturation," *IEEE Syst. J.*, vol. 16, no. 1, pp. 1114–1122, Mar. 2022.

[19] M. Saeedi, J. Zarei, R. Razavi-Far, and M. Saif, "Event-triggered adaptive optimal fast terminal sliding mode control under denial-of-service attacks," *IEEE Syst. J.*, vol. 16, no. 2, pp. 2684–2692, Jun. 2022.

[20] J. Chen et al., "Distributed control of multi-functional grid-tied inverters for power quality improvement," *IEEE Trans. Circuits Syst. I: Regular Papers*, vol. 68, no. 2, pp. 918–928, Feb. 2021.

[21] D. Senejohnny, P. Tesi, and C. De Persis, "A jamming-resilient algorithm for self-triggered network coordination," *IEEE Trans. Control Netw. Syst.*, vol. 5, no. 3, pp. 981–990, Sep. 2018.

[22] Z. Feng and G. Hu, "Secure cooperative event-triggered control of linear multiagent systems under DoS attacks," *IEEE Trans. Control Syst. Technol.*, vol. 28, no. 3, pp. 741–752, May 2020.

[23] A. Cetinkaya, K. Kikuchi, T. Hayakawa, and H. Ishii, "Randomized transmission protocols for protection against jamming attacks in multi-agent consensus," *Automatica*, vol. 117, 2020, Art. no. 108960.

[24] W. Li, H. Zhang, J. Zhang, and S. Sun, "Fully distributed event/self-triggered formation tracking for multiagent systems under denial-of-service attacks," *IEEE Syst. J.*, vol. 17, no. 4, pp. 5706–5713, Dec. 2023.

[25] A. Cetinkaya, H. Ishii, and T. Hayakawa, "An overview on denial-of-service attacks in control systems: Attack models and security analyses," *Entropy. Int. Interdiscipl. J. Entropy Inf. Stud.*, vol. 21, no. 2, 2019, Art. no. 210.

[26] *IEEE Standard for Interconnection and Interoperability of Distrib. Energy Resour. With Assoc. Electric Power Syst. Interfaces*, IEEE Std 1547-2018 (Revision of IEEE Std1547-2003), 2018.

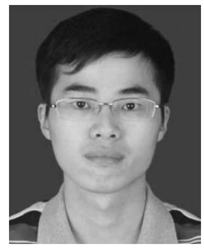

Shengxuan Weng received the B.S. degree in applied mathematics from the School of Mathematics and Statistics, Huazhong University of Science and Technology, Wuhan, China, in 2009, and the Ph.D. degree in automation from the School of Automation, Huazhong University of Science and Technology, in 2014.

He is currently an Associate Professor with the Institute of Advanced Technology, Nanjing University of Posts and Telecommunications, Nanjing, China. His research interests include distributed control, multiagent systems, and control approach in microgrid and smart grid.

Dong Yue (Fellow, IEEE) received the Ph.D. degree in control science and engineering from the South China University of Technology, Guangzhou, China, in 1995.

He is currently a Professor and the Dean of the Institute of Advanced Technology and the College of Automation and AI, Nanjing University of Posts and Telecommunications, Nanjing, China. He was a Changjiang Professor with the Department of Control Science and Engineering, Huazhong University of Science and Technology, Wuhan, China. His research interests include analysis and synthesis of networked control systems, multiagent systems, optimal control of power systems, and the Internet of Things.

Dr. Yue was a Co-Editor-in-Chief for IEEE TRANSACTIONS ON INDUSTRIAL INFORMATICS, an Associate Editor for IEEE INDUSTRIAL ELECTRONICS MAGAZINE and IEEE TRANSACTIONS ON SYSTEMS, MAN, AND CYBERNETICS: SYSTEMS, and a Guest Editor for Special Issue on New Trends in Energy Internet: Artificial Intelligence-Based Control, Network Security and Management for IEEE TRANSACTIONS ON SYSTEMS, MAN, AND CYBERNETICS: SYSTEMS.

Jianbo Chen received the B.S. and Ph.D degrees in automation from the College of Automation and AI, Nanjing University of Posts and Telecommunications, Nanjing, China, in 2015 and 2020, respectively.

He is currently a Lecturer with the Institute of Advanced Technology, Nanjing University of Posts and Telecommunications. His research interests include distributed control, event-triggered control, parallel control of multiple inverters, and power quality improvement of the microgrid.

Chunxia Dou (Senior Member, IEEE) received the B.S. and M.S. degrees in automation from the Northeast Heavy Machinery Institute, Qiqihaer, China, in 1989 and 1994, respectively, and the Ph.D. degree in electrical engineering from Yanshan University, Qinhuangdao, China, in 2005.

In 2010, she joined the Department of Engineering, Peking University, Beijing, China, where she was a Post-Doctoral Fellow for two years. From 2005 to 2019, she was a Professor with the School of Electrical Engineering, Yanshan University. Since 2019, she has been a Professor with the Institute of Advanced Technology, Nanjing University of Posts and Telecommunications, Nanjing, China. Her research interests include MAS-based control, event-triggered hybrid control, distributed coordinated control, multimode switching control, and their applications in power systems and smart grids.